Experimental Study of the Galloping Stability of H-Section Beams.

Gandia, F., Meseguer, J.**, Sanz-Andrés, A.***
** EUIT Aeronáutica, UPM (Universidad Politécnica de Madrid), Madrid, Spain.*
***IDR/UPM Universidad Politécnica de Madrid, Spain.*
fernando.gandia@upm.es, j.meseguer@upm.es, angel.sanz.andres@upm.es

Abstract

The phenomenon of self-induced vibrations, in cross-flow, of prismatic beams has been studied for decades, but it is still of great interest due to their important effects in many different industrial applications.

This paper presents the experimental study developed on a prismatic beam with H-section. The aim of this analysis is to add some additional insight on the behaviour of the flow around this type of section, in order to reduce the aerodynamic galloping, and even to avoid it. The influence of the most relevant geometrical parameters that define the H section on the galloping behaviour of these beams has been analysed by applying the Den Hartog criterion. Therefore, wind loads coefficients have been measured through wind tunnel tests. Besides, the morphology of the flow past the tested bodies has been visualised by using smoke visualization techniques.

Since the rectangular section beam is a limit case of the H-section configuration, the results here obtained concerning this configuration are compared with the ones published in the literature concerning rectangular configurations, the agreement being satisfactory.

1. Introduction

It is well known that two-dimensional bluff bodies in cross-flow are subject to typical aeroelastic phenomena like vortex shedding, translational and torsional galloping, and even flutter. Some of these phenomena can even appear coupled occasionally. Galloping is a typical instability of flexible, lightly damped structures. Under certain conditions these structures may have large amplitude, normal to wind oscillations, at much lower frequencies than those of vortex shedding found in the Kármán vortex street.

Although many two-dimensional bodies can experience galloping episodes, this kind of instability seems to appear rather in bluff bodies than in streamlined ones. Therefore galloping used to be considered as a phenomenon associated to non-aeronautical engineering, were bluff bodies are largely used. However, galloping episodes have been reported in aerospace applications, as it was the case of the liquid oxygen cable tray on the liquid-oxygen tank of the Space Shuttle launch vehicle, which at transonic flight speeds was exposed to high velocity cross flow, generated by the bow shock from the strapped-on solid rocket booster [1-3].

Theoretical foundations of galloping are well established and can be easily understood through an extremely simple

theory like the one due to Den Hartog [4], which, in a first attempt, is enough to elucidate if a given two-dimensional body can gallop or not. According to Den Hartog, galloping can be explained by taking into account that, even if the incident wind velocity U_∞ is uniform and constant, in a body reference frame the lateral oscillation of the body can cause that the total velocity experiences changes both in its magnitude and direction with time. Therefore, the body angle of attack also changes with time, hence the aerodynamic forces acting on it (figure 1).

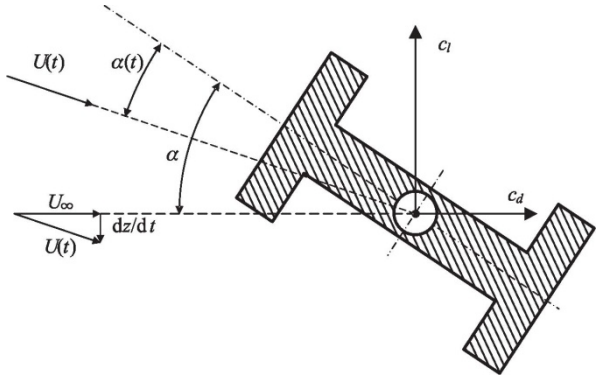

Figure 1. Sketch of a typical H beam under galloping. U_∞ is the unperturbed upstream flow velocity, dz/dt is the vertical velocity due to transversal body oscillation, α is the angle of attack of the body under static conditions, and $\alpha(t)$ the actual one. Lift and drag coefficients are c_l and c_d, respectively.

Concerning the stability analysis, it is based on the simplest model of galloping (one degree of freedom) it is assumed that a two-dimensional body, whose mass per unit length is m, is elastically mounted on a support with a damping coefficient ζ and a stiffness $m\omega^2$ (where ω is the angular natural frequency). Within this approximation, if the aerodynamic force (proportional in this case to dz/dt) is considered as a contribution to the total damping of the system, the total damping coefficient is:

$$\zeta_T = \zeta + \frac{\rho U_\infty b}{4m\omega}\left(\frac{\mathrm{d}c_l}{\mathrm{d}\alpha} + c_d\right), \tag{1}$$

where U_∞ stands for the upstream flow velocity, and b for a transversal characteristic length of the body (figure 2). Therefore, the oscillation will be damped if $\zeta_T > 0$ and unstable if $\zeta_T < 0$. As the mechanical damping ζ is generally positive, instability will only occur if the parameter $H = \mathrm{d}c_l/\mathrm{d}\alpha + c_d < 0$, expression known as Den Hartog criterion, which is a necessary condition for galloping instability. The sufficient condition for galloping is $\zeta_T < 0$, or, according to equation (1) and the above definition of the parameter H, $H < -4m\zeta\omega/(\rho U b)$. Note that in this last expression the second member tends to zero when the wind velocity increases, which means that the possibility of galloping becomes higher as the wind velocity increases.

From inspection of equation (1), since the drag coefficient is positive, it is clear that the slope of the lift coefficient versus angle of attack curve must be negative, which means that the body must be stalled ($\mathrm{d}c_l(\alpha)/\mathrm{d}\alpha < 0$) and that the absolute value of this slope curve must be larger than the drag coefficient.

Galloping has focused the attention of many researchers during the last decades because of its impact in very common problems related to ice accretion on electric transmission lines, traffic signal gantries and structures, catenary leads, and many other two-dimensional configurations, and a fairly large number of papers dealing with the

galloping properties of a wide spectrum of geometries has been published (see [5-9] for rewiews on this topic). It must be pointed out that most of the effort in galloping research has been concentrated in bodies with square or rectangular cross-sections, although prismatic bodies with other cross-sectional shapes have been also considered [10-14].

In the last years some research on galloping has been carried out at IDR/UPM, and a systematic parametric analysis of simple cross-section two-dimensional bodies has been accomplished (the geometries analysed up to now are isosceles triangular cross-sections, as well as biconvex and rhomboidal cross-sections). In this paper the transverse galloping characteristics of H shaped beams is analysed through static aerodynamic tests, measuring aerodynamic forces on the models. It must be noted that other aeroelastic phenomena could also be possible in this type of bodies, but they cannot be analysed in a quasi-static approach. The aim of this study is to elucidate how the body geometry affects the galloping characteristics (figure 2), as well as the analysis of suitable geometry modifications to suppress galloping phenomena.

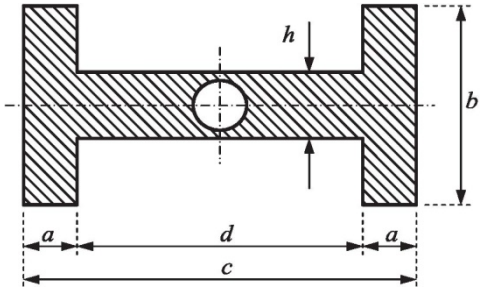

Figure 2. Parameters that define the geometry of a typical H beam.

2. Experimental setup and procedures

Tests were performed at the Laboratorio de Aerodinámica of the E.U.I.T. Aeronáutica (Universidad Politécnica de Madrid). An open return, blown, Plint & Partners modified wind tunnel was used. It has a 8:1 contraction ratio and a rectangular test chamber of 160 mm wide, 1200 mm high and 1500 mm length. The speed in the test section can be up to 30 m/s, driven by an AC motor of 23 kW, connected to a centrifugal fan.

The turbulence intensity level is 0.7 %, and the non-uniformity of the flow less than 1 %, so that this wind tunnel becomes appropriate for low Reynolds number tests [15].

For the aerodynamic forces measurement, an external, pyramidal, three components, electronic Plint Ltd. balance was used, which allow the lift and drag force to be measured, as well as the pitching moment of the body placed inside the test chamber. Measurements require the subtraction of the initial values and the results are then multiplied by the calibration constants of each load cells.

Dynamic pressure inside the test chamber is measured by a standard Pitot tube attached to the top wall of the wind

tunnel, just ahead of the model, and connected to an MP6KS Air Ltd. pressure transducer. From Pitot tube measurement, taking into account the temperature and ambient pressure at the laboratory, the air flow velocity U_∞ is obtained, leading to a Reynolds number, $\mathrm{Re} = U_\infty c/\nu \cong 10^5$, where c stands for the body chord, as defined in figure 2, and ν for the kinematic viscosity of air.

All the electrical signals coming from the wind tunnel are acquired by a HP 6110 laptop, through a National Instruments DAQ Card–6062 E with 16 analogical input channels.

Before a tests campaign, some previous tests were made, both at low and high angles of attack, to determine the optimum frequency rate and the sampling time.

The different models were made of Necuron® resin and machined in a Roland MDX–540 milling machine with a 0.1 mm precision. All of them are 158 mm span, thus leaving a 1 mm gap between the wind tunnel walls and the lateral surfaces of the models. It must be pointed out that this gap does not affect to the two-dimensional behaviour of the model, the reasons being that these gaps are very narrow and they are placed at the boundary layers that develop at the wind tunnel walls [16]. Bodies are fixed to the balance through a 12 mm steel rod, placed at the centre of mass of the models, as sketched in figure 1.

Besides, some visualization tests were performed by using a small smoke wind tunnel (the working section is 0.4 m high, 0.04 m wide and 0.6 m long), in order to get additional information on the morphology of the flow past the models.

In experiments the lift, $l(\alpha)$, drag, $d(\alpha)$, and pitching moment, $m(\alpha)$, were measured at angles of attack varying form $\alpha = 0^\circ$ to $\alpha = 90^\circ$ at variable $\Delta\alpha$ step (this step is smaller, $\Delta\alpha = 1^\circ$, where the lift slope curve is negative, and galloping can occur, and larger, $\Delta\alpha = 5^\circ$, where the lift slope is positive). From measured results the aerodynamic coefficients are determined, $c_l(\alpha) = l(\alpha)/(q_\infty c)$, $c_d(\alpha) = d(\alpha)/(q_\infty c)$, $c_m(\alpha) = m(\alpha)/(q_\infty c^2)$, and then the Den Hartog parameter $H = \mathrm{d}c_l/\mathrm{d}\alpha + c_d$ is calculated.

3. Experimental results

Two types of H-section beam configurations were considered. In all cases the lengths c and b were kept constant. In the first type, type I, the length a was varied from $a/c = 0.015$ to $a/c = 0.50$ (this last configuration corresponds to a rectangular beam), the aim of these tests being to study the influence of thickness of the extreme vertical plates on the galloping behaviour.

In the second set of H beam configurations, type II, the thickness a was kept constant ($a/c = 0.015$), but holes of different diameters were drilled on the vertical plates to modify its porosity. The porosity is defined as the ratio to the frontal surface of the drilled portion of the vertical plates, that is $(b - h)s$, were s stands for the model span, of the

surface of the holes made in such a surface, $\phi = \pi nr^2/[(b - h)s]$, n being the number of holes made in the span s and r the hole radius.

The results obtained with the type I beams are depicted in the left column of figure 3, whereas results corresponding to porous H beams (type II) are shown in the right column of the same figure 3.

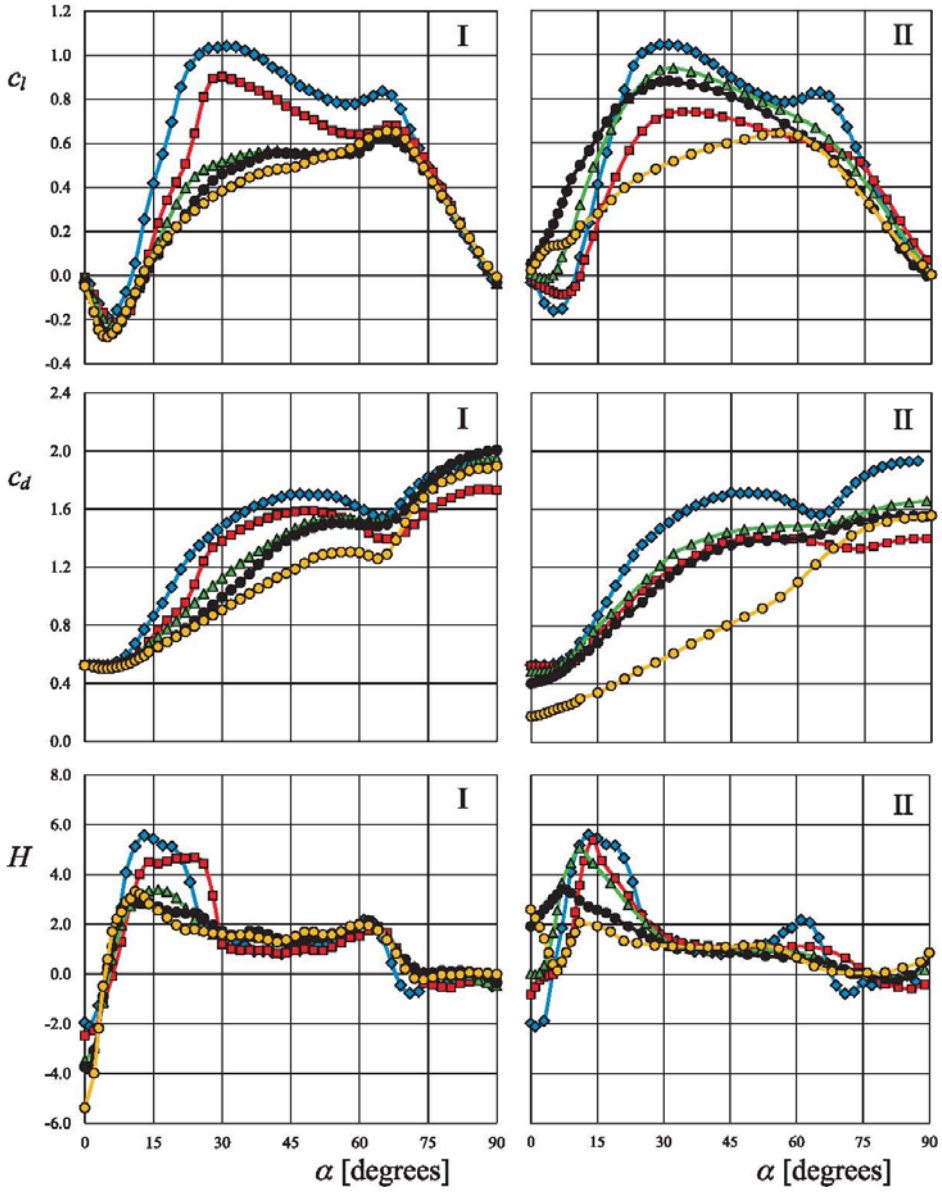

Figure 3. Variation with the angle of attack, α, of the lift coefficient, c_l, the drag coefficient, c_d, and the Den Hartog parameter $H = dc_l/d\alpha + c_d$. Left column, type I H beams (solid vertical plates) with different $2a/c$ ratio (the symbols identify the values of the parameter $2a/c$ according to the key: $2a/c = 1$, yellow circles; $2a/c = 0.8$, black circles; $2a/c = 0.6$, green triangles; $2a/c = 0.2$, red squares; $2a/c = 0.03$, blue rhombi). Right column, type II H beams, with fixed $2a/c = 0.03$ and $b/c = 0.5$ values, but with vertical plates with different porosities (the symbols identify the values of the parameter ϕ according to the following key: $\phi = 1$, yellow circles; $\phi = 0.6$, black circles; $\phi = 0.4$, green triangles; $\phi = 0.2$, red squares; $\phi = 0$, blue rhombi).

Concerning type I beams, the results show that the lift slope becomes negative close to $\alpha = 0^o$ until it reaches a minimum at $\alpha \cong 6^o$ (the beam is stalled), this behaviour being the same independently of the value of the parameter $2a/c$, beyond this minimum the lift coefficient start to grow as the angle of attack grows, so that the lift coefficient slope curve becomes positive. Form the point of view of galloping there is another region, close to $\alpha = 90^o$, where the lift slope becomes again largely negative.

The drag coefficient increases as the angle of attack grows in almost all the whole range ($0^o \leq \alpha \leq 90^o$) except close to $\alpha \cong 65^o$ where relative minima appear no matter the value of the parameter $2a/c$ is. These local minima coincide with the angles of attack where the lift slopes start to be almost constant and largely negative (figure 3).

To get some additional insight on this behaviour some visualization in a small smoke wind tunnel were performed, and some of the pictures obtained are shown in figure 4. Note that for $\alpha < 55^o$ the upper boundary layer separates at the upper leeward corner of the H beam, whereas for $\alpha > 75^o$ the separation takes place at the upper windward corner. For $\alpha \cong 65^o$ smoke streamlines are parallel to the H beam upper surface, which probably implies a narrow wake behind the body at these values of the angle of attack.

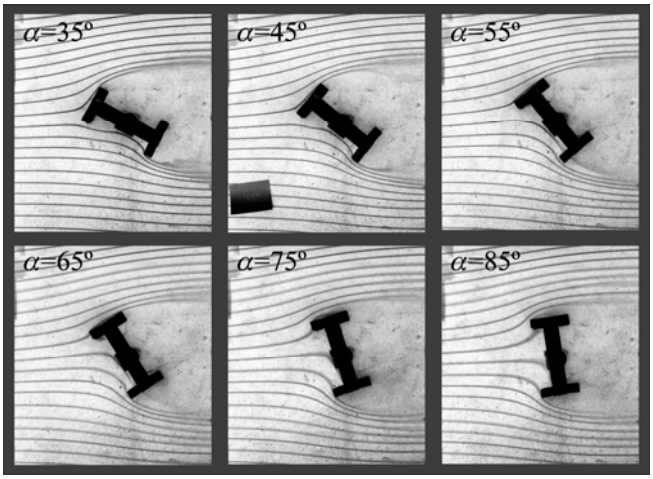

Figure 4. Smoke visualization of the flow past a H beam with geometrical parameters $2a/c = 0.25$ and $b/c = 0.45$.

With the experimental results related to c_l and c_d, the Den Hartog function $H = dc_l/d\alpha + c_d$ has been determined, and represented in figure 3. As it can be observed, there is a region close to $\alpha = 0^o$ where H beam configurations are unstable (see also figure 5), and there is another region close to $\alpha = 90^o$ where these bodies are weakly unstable. Between these two regions H beams are not prone to transversal galloping oscillations. It must be remarked that for large values of the angle of attack, although according to Den Hartog criterion the H function is negative, the absolute values of this parameter are so small that the resulting motions are only marginally unstable. Note also that the size of this region decreases as the parameter a grows, until a given critical value of this parameter is reached. The size of the unstable region increases as the parameter a grows beyond the critical value.

Note that the unstable region must be almost the same for $2a/c = 0$ and $2a/c = 1$, provided the chord c is large enough (in both cases the H beam behaves as a rectangular cross section body).

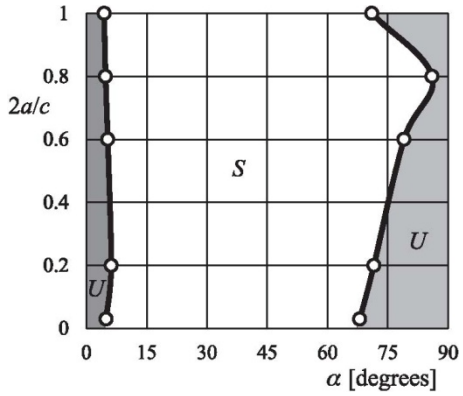

Figure 5. Stability diagram of H-section beams in the H geometry versus angle of attack plane ($2a/c$ vs. α plane), where the lengths a and c are defined in figure 1. Shadowed areas indicate unstable regions, although the right hand side region is only marginally unstable.

The differences between the tested type II H beams are in the porosity ϕ of the vertical plates (when $\phi = 0$º), which was changed from $\phi = 0$ (solid vertical plates, yellow circles in the right column of figure 3) to $\phi = 1$ (no vertical plates, blue rhombi). The measured results, c_l, c_d and H versus ϕ are shown in figure 3. According to these plots, it seems that H beams are stable for large enough values of the porosity, both for small and large values of the angle of attack (figure 6)

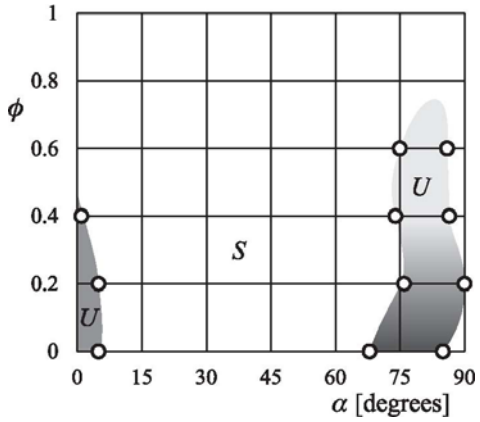

Figure 6. Stability diagram of H beams in the porosity versus angle of attack plane (ϕ vs. α plane). The results correspond to H beams with $2a/c = 0.03$ and $b/c = 0.45$, where the lengths a, b and c are defined in figure 2. Shadowed areas indicate unstable regions, although the right hand side region is only marginally unstable. Note that for large values of the porosity, H beams are not unstable.

Gallop absence for large porosities, say greater than $\phi = 0.4$, can be explained by the fact that the central core of the H section, without the vertical plates, is a rectangular section with $h/d = 0.25$ (see figure 2) which is no prone to gallop [8].

The measured results for type II H beams show a behavior similar to type I with $2a/c = 0.03$, but as the porosity tends to 1, the curves progressively approach the behavior of rectangular section with $h/d = 0.25$

4. Conclusions

This paper describes an experimental procedure to analyse the influence of several geometric parameters on the galloping behaviour H cross-section beams. A wind tunnel was used to measure the aerodynamic coefficients of lift, c_l, and drag, c_d, at angles of attack from 0 to 90º, and then the Den Hartog criterion was applied. In order to improve the understanding of the physical behavior of the air flow around the section, additional visualization tests on a smoke wind tunnel was also performed.

Although the analysis has been constrained to a few geometrical configurations, experimental results show that, for the configuration under study, the influence of the parameter $2a/c$ do not substantially affects the phenomenon of galloping. On the other hand, porosity, ϕ, seems to be an important parameter to effectively control the galloping behaviour.

References

1. **Ericsson, L.E. and Reding, J.P.** 1982. *Aeroelastic Stability of Space Shuttle Protuberances,* Journal of Spacecraft, Vol. 19, pp. 307-313.
2. **Reding, J.P. and Ericsson, L.E.** 1982. *Analysis of Static and Dynamic Wind Tunnel Tests of the Shuttle Cable Trays*, Journal of Spacecraft, Vol. 19, pp. 412-418.
3. **Orlik-Rückemann, K.J. and LaBerge, J.G.** 1983. *Dynamic Wind Tunnel Tests of the Simulated Shuttle External Cable Trays*, Journal of Spacecraft and Rockets, Vol. 20, pp. 5-10.
4. **Den Hartog, J.P.** *Mechanical Vibrations, 4th ed.*, McGraw-Hill, New York, 1956.
5. **Blevins, R.D.** 1990. *Flow-Induced Vibrations, 2nd ed*. Krieger Publishing Co. Malabar, Florida, 1990.
6. **Naudascher, E. and Rockwell, D.** *Flow-Induced Vibrations: An Engineering Guide.* A.A. Balkema, Rotterdam, 1994.
7. **Hémon, P. and Santi, F.** 2002. *On the Aeroelastic Behaviour of Rectangular Cylinders in Cross-flow.* Journal of Fluids and Structures, Vol. 16, pp. 855-889.
8. **Païdoussis, M. Price, S. and de Langre, E.** *Fluid–Structure Interactions: Cross-Flow-Induced Instabilities*, Cambridge University Press, 2011.
9. **Alonso, G., Sanz-Lobera, A. and Meseguer, J.** 2012. *Hysteresis Phenomena in Transverse Galloping of Triangular Cross-Section Bodies*. Journal of Fluids and Structures, Vol. 33, pp. 243–251.
10. **Alonso, G., Meseguer, J. and Perez-Grande, I.** 2005. *Galloping Instabilities of Two-Dimensional Triangular Cross-Section Bodies*. Experiments in Fluids, Vol. 38, pp. 789–795.

11. **Alonso, G., Valero, E. and Meseguer, J.** 2009. *An Analysis on the Dependence on Cross Section Geometry of Galloping Stability of Two-Dimensional Bodies Having either Biconvex or Rhomboidal Cross Sections.* European Journal of Mechanics B/Fluids, Vol. 28, pp. 328–334.
12. **Chen, Z.-Q., Liu, G.-D. and Liu, M.-G.** *Wind-Resistant Characteristics of H-Shape Slender Hangers*, 7th Asia-Pacific Conference on Wind Engineering, Taipei, Taiwan, 2009.
13. **Alonso, G., Meseguer, J., Sanz-Andrés, A. and Valero, E.** 2010. *On the Galloping Instability of Two-Dimensional Bodies Having Elliptical Cross Sections*. Journal of Wind Engineering and Industrial Aerodynamics, Vol. 98, pp. 438-448.
14. **Joly, A., Etienne, S. and Pelletier, D.** 2012. *Galloping of Square Cylinders in Cross-Flow at Low Reynolds Numbers.* Journal of Fluids and Structures, Vol. 28, pp. 232–243.
15. **Barlow, J.B., Rae, W.H. and Pope, A.** *Low-Speed Wind Tunnel Testing, 3rd ed.* John Wiley & Sons Inc., New York, 1999.
16. **Ayuso, L., Sant, R. and Meseguer, J.** 2013. *Influence of Leading Edge Imperfections on the Aerodynamic Characteristics of NACA 63(2)215 Laminar Aerofoils at Low Reynolds Number*, Proceedings IMechE, Part G: Journal of Aerospace Engineering. DOI 10.1177/0954410013481418